Stabilization of Cu^{+} by tuning CuO-CeO_2 interface for selective electrochemical CO_2 reduction to ethylene

Senlin Chu,[a,#] Xupeng Yan,[b,#] Changhyeok Choi,[c,#] Praveen Kolla,[d,*] Song Hong,[a] Alex W. Robertson,[e] Justus Masa,[f] Buxing Han,[b] Yousung Jung[c,*] and Zhenyu Sun[a,*]

ABSTRAT: Electrochemical conversion of carbon dioxide (CO2) into multi-carbon fuels and chemical feedstocks is important but remains challenging. Here, we report the stabilization of Cu+ within a CuO–CeO2 interface for efficient and selective electrocatalytic CO2 reduction to ethylene under ambient conditions. Tuning the CuO/CeO2 interfacial interaction permits dramatic suppression of proton reduction and enhancement of CO2 reduction, with an ethylene faradaic efficiency (FE) as high as 50.0% at −1.1 V (vs. the reversible hydrogen electrode) in 0.1 M KHCO3, in stark contrast to 22.6% over pure CuO immobilized on carbon black (CB). The composite catalyst presents a 2.6-fold improvement in ethylene current compared to that of CuO/CB at similar overpotentials, which also exceeds many recently reported Cu-based materials. The FE of C2H4 remained at over 48.0% even after 9 h of continuous polarization. The Cu+ species are believed to be the adsorption as well as active sites for the activation of CO2 molecules, which remain almost unchanged after 1 h of electrolysis. Further density functional theory calculations demonstrate the preferred formation of Cu+ at the CuO–CeO2 interface. This work provides a simple avenue to convert CO2 into high-value hydrocarbons by rational stabilization of Cu+ species.

INTRODUCTION

Electrochemical carbon dioxide (CO_2) reduction (ECR) shows promise in reducing greenhouse gas emissions and storing intermittent renewable electricity, as well as attaining energy security and sustainability.[1, 2] Although this energy conversion process can be conducted under mild temperature and pressure, there are still many challenges such as low conversion efficiency and poor product selectivity that have to be overcome.[3, 4] To enable progress towards this goal, the development of catalysts with high efficiency, sufficient selectivity, and low cost is necessary.[5, 6] The synthesis of valuable hydrocarbons and other chemicals through ECR has drawn significant

attention as a potential scheme for recycling of CO_2.[7-16] In particular, C_{2+} (containing two or more carbon atoms) compounds such as ethylene have high energy densities and enjoy global demand in comparison to C_1 products.[17, 18] For instance, ethylene is widely used as an industrial feedstock for manufacturing plastics and diesel, and its selective production in lieu of methane is important.

Copper, with its unique electronic properties, has been shown to stabilize a CO intermediate (*CO), and enable it to be further reduced to multi-carbon products via CO dimerization to yield an *OCCO adsorbate and subsequent hydrogenations.[17] However, Cu is intrinsically limited by the scaling relations between the binding energies of various reaction intermediates on the metallic surfaces, which leads to wide product distributions and undesirable hydrogen evolution, thus hampering large-scale practical implementation.[19] Selective reduction of CO_2 into industrially important C_{2+} species remains an ongoing challenge. Recent investigations indicate that preferential conversion of CO_2 to C_{2+} products can be achieved using Cu-based materials doped with foreign atoms,[20] Cu alloys,[21, 22] or through control of exposed crystal lattice,[23, 24] oxidation state,[25, 26] and surface morphology.[27-30] For example, single-crystal Cu (100) was demonstrated to display good selectivity for ethylene evolution with a faradaic efficiency (FE) of about 40.0%, which can be further improved to 50.0% over Cu (711) at -5.0 mA cm^{-2} in 0.1 M $KHCO_3$.[30] A recent study showed that CuAg bimetallic catalysts have enhanced selectivity to C_{2+} products, which was attributed to a suppression of the hydrogen evolution reaction (HER) due to the formation of compressively strained CuAg surface alloys.[31] In addition, Cu/oxide interfaces are regarded to be critical to inhibit the parasitic HER during electrocatalytic CO_2 reduction.[32, 33] Oxides of copper exhibit enhanced ECR activity and increased selectivity towards multi-carbon products. The selectivity of these catalysts is dependent on copper oxidation state.[29] Some computational studies have suggested that the coexistence of a Cu^+/Cu^0 mixture synergistically promotes CO_2 reduction to C_{2+} products due to improved CO_2 activation and CO dimerization.[34, 35] Experimentally, however, evidence of the stability of the active Cu^+ species during CO_2 reduction remains unclarified thus far.

Herein, we report on the stabilization of Cu^+ by controlling the interplay between lattice-mismatched CuO and CeO_2. This scheme allows one to design an efficient and selective catalyst for electrocatalytic CO_2 reduction to produce ethylene, among other products (methane, carbon monoxide). Catalytic selectivity can be greatly improved by taking advantage of CuO-CeO_2 interactions in different composition regimes and

interfacial structures. A remarkable FE for ethylene production of up to 50.0% was obtained at mild overpotentials, outperforming many previously reported Cu-based electrocatalysts. Furthermore, density functional theory (DFT) calculations revealed that CeO_2 changes the oxidation state of Cu atoms toward Cu^+ at the CuO-CeO_2 interface.

RESULTS AND DISCUSSION

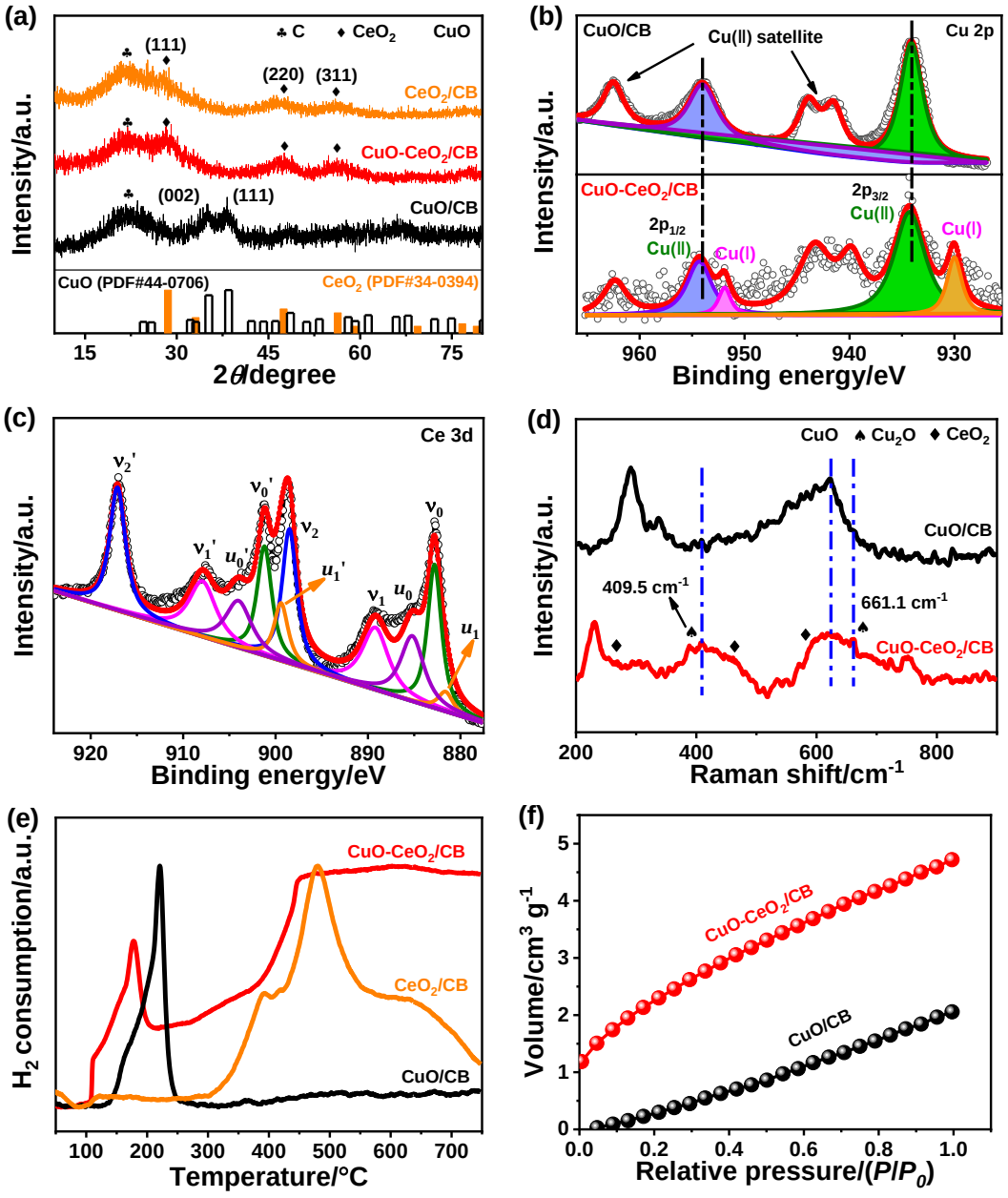

Figure 1. (a) XRD patterns of CeO_2/CB, CuO/CB, and CuO-CeO_2/CB. (b) Cu 2p XPS spectra of CuO/CB and CuO-CeO_2/CB. (c) Ce 3d XPS spectrum of CuO-CeO_2/CB. (d) Raman spectra of

CuO/CB and CuO-CeO_2/CB. (e) H_2-TPR profiles of CeO_2/CB, CuO/CB, and CuO-CeO_2/CB. (f) CO_2 adsorption curves of CuO/CB and CuO-CeO_2/CB.

The X-ray diffraction (XRD) patterns of CuO-CeO_2/CB together with individual CuO/CB and CeO_2/CB are shown in Fig. 1a. Apart from a broad peak at 22.2º, originating from carbon black with low crystallinity, diffraction peaks at about 28.1, 47.6 and 56.0º were observed in both CeO_2/CB and CuO-CeO_2/CB, corresponding to the (111), (220), and (311) planes of CeO_2 (PDF# 34-0394). These indicate the formation of fluorite ($Fm\bar{3}m$) CeO_2 with a face-centered cubic (*fcc*) structure in the composites. Unlike the bare CuO/CB that displayed representative monoclinic CuO peaks (PDF# 44-0706), no diffraction peaks of any Cu compounds were discernible in the XRD pattern of CuO-CeO_2/CB, likely due to the low loading and/or small size of CuO in the composite.

X-ray photoelectron spectroscopy (XPS) was employed to acquire information about the surface composition and chemical state of the Cu species, as well as possible interactions between copper and cerium oxides. Fig. 1b shows the Cu 2p signal of CuO/CB and CuO-CeO_2/CB. The Cu 2p core-level spectrum of CuO/CB reveals pronounced CuO features, that is, Cu $2p_{1/2}$ and $2p_{3/2}$ peaks with binding energies (BEs) at 954.0 and 934.0 eV, respectively. Strong Cu^{2+} satellites at 962.6, 944.0, and 941.6 eV were also clearly observed.[36] Nevertheless, no apparent peaks assigned to Cu^+ can be identified. In contrast, two peaks located at 954.3 and 951.9 eV were observed in CuO-CeO_2/CB, which can be attributed to Cu^{2+} $2p_{1/2}$ and Cu^+ $2p_{3/2}$, respectively.[10] This unambiguously verifies the formation and stabilization of Cu^+, likely owing to electron transfer from Ce^{3+} to Cu^{2+}. The Cu^+ percentage was determined to be 19.7% in CuO-CeO_2/CB, based on the peak area ratio of all copper oxidation states in the Cu 2p and LMM regions. Fig. 1c depicts the Ce 3d signals of CuO-CeO_2/CB having a satellite structure due to hybridization of Ce 3d orbitals with O 2p orbitals and partial occupancy of the 4f levels.[37] The $3d_{5/2}$ and $3d_{3/2}$ spin-orbit components (spin-orbit splitting, ~18.5 eV) are denoted as ν and ν′, respectively, which are in line with the previous literature on Ce(IV).[38] The peaks of ν_0 and ν_1 were attributed to a mixing configuration of the $3d^9$ $4f^2$ (O $2p^4$) and $3d^9$ $4f^1$ (O $2p^5$) Ce^{4+} states and ν_2 to the $3d^9$ $4f^0$ (O $2p^6$) Ce^{4+} state.[36] The same assignment could be applied to the ν′ structures, which correspond to the Ce $3d_{3/2}$ level. This illustrates the major valence of Ce(IV) in the sample, consistent with the XRD result. Four peaks u_0 (BE ≈ 885.8 eV), u_1 (BE ≈ 880.6 eV), u_0' (BE ≈ 904.1 eV), and u_1' (BE ≈ 899.5 eV)

associated with Ce^{3+} were identified, indicating the presence of Ce_2O_3 in the sample.[39] The well-defined peak ν_2' typical of Ce^{4+} can be used to estimate the fraction of Ce^{4+}.[40] Given that the area of the ν_2' component comprises 14.0% of the overall area of the Ce 3d region, the Ce^{3+} percentage was estimated to be 27.0%. The deconvoluted O 1s XPS spectrum of CuO-CeO_2/CB (Fig. S1) displays a predominant peak at 529.7 eV arising from lattice oxygens in the metal oxides, and two less intense peaks at 531.2 and 532.6 eV that can be assigned to defective sites (surface oxygen vacancies) and physisorbed water, respectively.

The presence of Cu^+ in CuO/CeO_2 heterostructure was also evidenced by Raman scattering experiments. The bands centered at about 258.0, 462.9, and 595.0 cm^{-1} were identified in Fig. 1d, which can be well assigned to the F_{2g} mode, second-order transverse acoustic (2TA) mode, and defect-induced (D) mode of fluorite CeO_2, respectively.[41] It is noteworthy that the three peaks at 290.4, 337.0 and 622.8 cm^{-1} that appeared for CuO/CB, are attributed to the respective single A_g mode and two B_g optical modes of cupric oxide.[42] However, for CuO-CeO_2/CB, the feature around 290.4 cm^{-1} disappeared and a new band at 230.4 cm^{-1} was observed being tentatively assigned to one-magnon scattering, which arose from the antiferromagnetic ordering of the Cu^{2+} ions.[42] A further two distinct peaks at 409.5 and 661.1 cm^{-1} are observable, typical of Cu^+ Raman fingerprints.[42] This further confirms that CuO was partially converted to Cu_2O, possibly induced by adjacent CeO_2 nanoparticles. These results are consistent with the XPS data in Fig. 1b.

Temperature-programmed reduction by hydrogen (H_2-TPR, Fig. 1e) manifested two marked H_2 consumption peaks at 110.0 and 178.0 °C for CuO-CeO_2/CB, being ascribed to the reduction of the subsurface $Cu^{\delta+}$ to Cu^+ and further to Cu^0 respectively, by consuming reducible oxygen from the CuO_x species. Notably, the TPR reduction peaks shifted to lower temperatures relative to CuO/CB, which is likely a result of hydrogen spillover to CuO at the CuO/CeO_2 interface. Furthermore, the CuO-CeO_2/CB exhibited a CO_2 uptake capacity of 4.7 cm^3 g^{-1} (Fig. 1f), 2.3 fold as large as that of CuO/CB. This could lead to enriched CO_2 on the local surface of the working electrode, thus boosting *CO coverage and dimerization. The significant enhancement in CO_2 capture ability is due to the introduction of CeO_2, which can effectively adsorb CO_2, forming carbonates and hydrogen carbonates. It can be envisioned that the as-made hybrid catalyst may facilitate multiple interesting functionalities such as adsorption, electronic, activation, and catalysis, among others, based on the synergistic interaction between CuO and CeO_2.

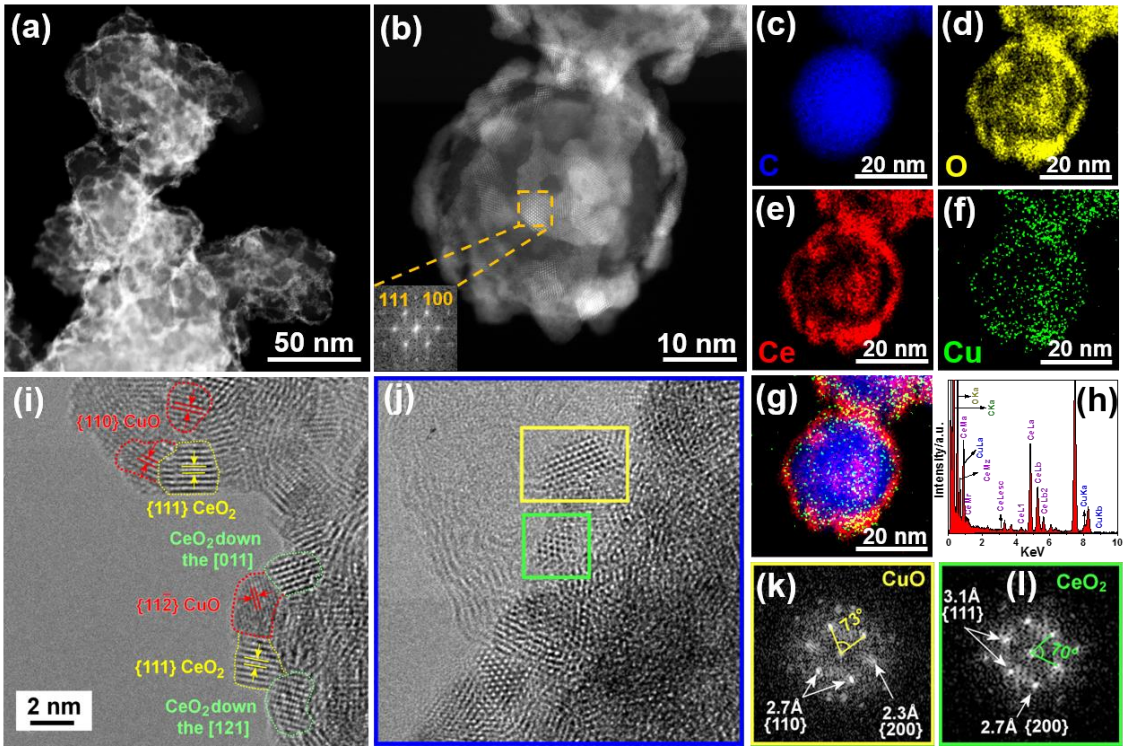

Figure 2. (a-b) HAADF-STEM images of CuO-CeO_2/CB. The inset in image (b) shows the corresponding FFT of CuO-CeO_2/CB. EDS elemental maps of (c) C, (d) O, (e) Ce, (f) Cu, and (g) overlay of C (blue), Ce (red) and Cu (green) over the region shown in image (b), along with corresponding EDS spectrum (h). (i) HRTEM image of CuO-CeO_2/CB. (j-l) Magnified image of the blue rectangle in image (i) and FFTs of the regions encased by the yellow and green rectangles in image (j).

To decipher the morphological features of our catalyst, aberration corrected high-angle annular dark-field scanning transmission electron microscopy (HAADF-STEM) was performed on CuO-CeO_2/CB. Fig. 2a,b showed the formation of many reticular nanoparticles (NPs) homogeneously distributed on carbon black. The (111) and (100) planes of CeO_2 were indexed with the aid of fast Fourier transformation (FFT) (inset of Fig. 2b). Furthermore, the energy-dispersive X-ray spectroscopy (EDS) maps (Fig. 2c-g) along with the EDS spectrum (Fig. 2h) confirmed that the NPs were composed of CuO and CeO_2 crystallites. EDS elemental mapping revealed almost full overlap of Cu-rich and Ce-rich domains, indicating large interfaces between the two metal oxides. The crystallite sizes of CuO and of CeO_2 were found to be similar with sizes of less than 5 nm by high-resolution TEM (Fig. 2i,j). By FFT, *fcc* CuO and CeO_2

NPs were discerned (Fig. 2k,l). Most of the CuO crystals exhibited faceted cuboidal morphology and were surrounded by CeO_2 NPs (Fig. 2i,j).

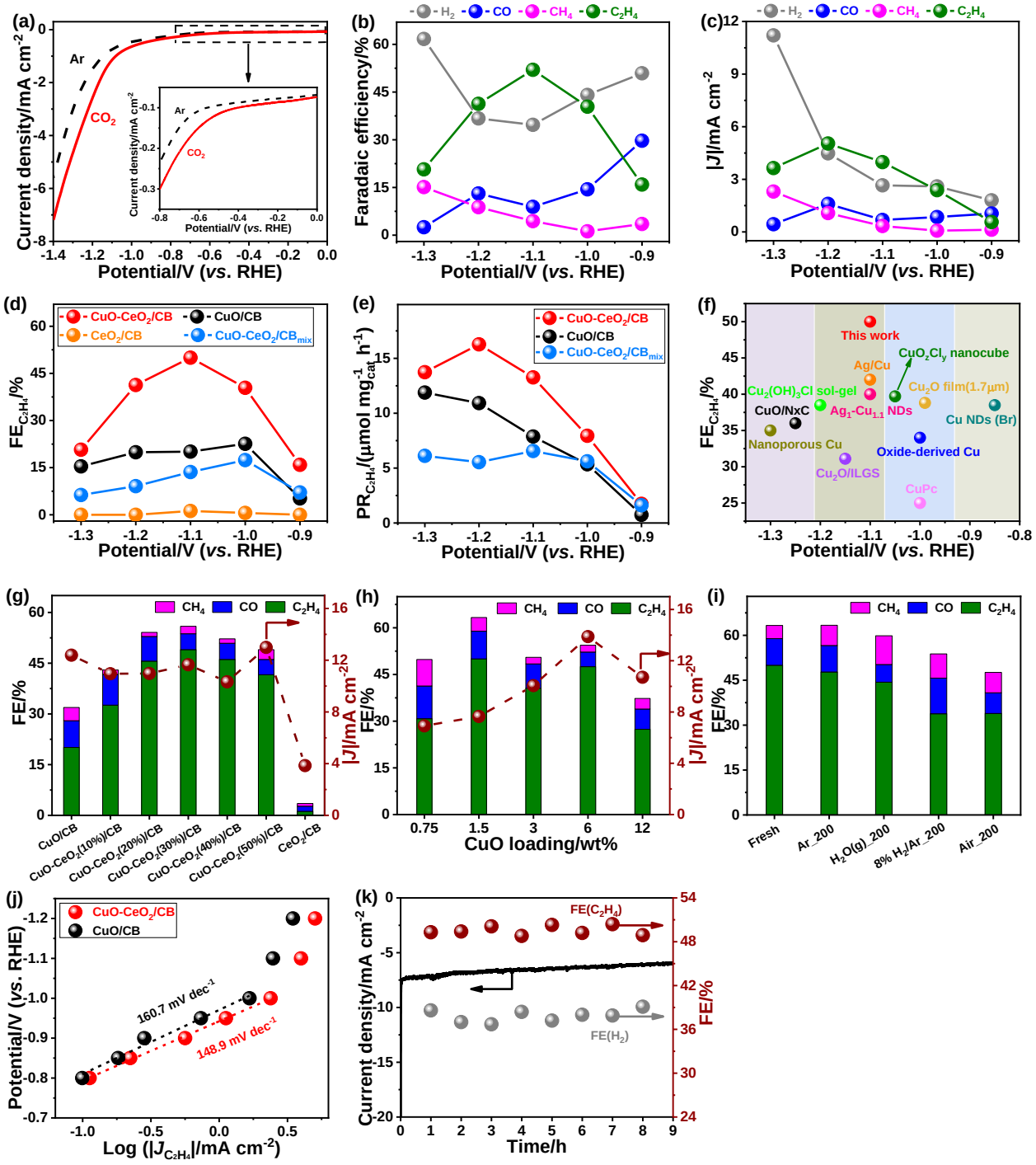

Figure 3. (a) LSV results of CuO-CeO_2/CB on a glassy carbon electrode in Ar- (dashed black line) or CO_2 (solid red line)-saturated 0.1 M $KHCO_3$ solutions at a scan rate of 5 mV s^{-1}. (b) Faradaic efficiencies and (c) partial current densities for ECR products over CuO-CeO_2/CB at various applied potentials. (d) C_2H_4 FEs of CuO-CeO_2/CB, CuO/CB, CeO_2/CB, and CuO-CeO_2/CB_{mix} in the potential range from −0.9 to −1.3 V. (e) Production rates of C_2H_4 at different potentials over

$CuO\text{-}CeO_2/CB$, CuO/CB, and $CuO\text{-}CeO_2/CB_{mix}$. (f) C_2H_4 FEs of $CuO\text{-}CeO_2/CB$ and other reported Cu-based electrocatalysts. FE and current density at −1.1 V (vs RHE) as a function of (g) CeO_2 loading at a fixed CuO content of 1.5 wt% and (h) CuO loading at a constant CeO_2 loading of 30.0 wt%. (i) FEs at −1.1 V (vs RHE) over fresh and treated $CuO\text{-}CeO_2/CB$ under Ar, H_2O, 8.0% H_2/Ar, and air. (j) Tafel plots of the partial current density for C_2H_4 production over $CuO\text{-}CeO_2/CB$, CuO/CB, and $CuO\text{-}CeO_2/CB_{mix}$. (k) Current-, C_2H_4 FE-, and H_2 FE-time responses of $CuO\text{-}CeO_2/CB$ at −1.1 V (vs RHE).

ECR is very sensitive to operating conditions, such as the nature and properties of the electrocatalyst, electrolyte composition, and electrochemical cell type. To evaluate the intrinsic catalytic properties of the as-prepared hybrids, we conducted the ECR in CO_2-saturated 0.1 M $KHCO_3$ aqueous electrolyte (pH 6.8) using a reported design of liquid H-type cell with continuous CO_2 bubbling.[43] The potential-dependent geometric current densities of $CuO\text{-}CeO_2/CB$ within the potential range of 0.0 to −1.4 V (vs RHE) were recorded by linear sweep voltammetry (LSV), as shown in Fig. 3a. Significantly higher cathodic currents were observed in a CO_2 environment than in an Ar environment within the entire potential region. CO, H_2, CH_4, HCOOH, and C_2H_4 were detected at applied potentials ranging from −0.9 to −1.3 V (vs RHE) in a CO_2-saturated 0.1 M $KHCO_3$ solution. The ECR preferably occurred over HER in the potential range from −0.9 to −1.2 V (vs RHE), while HER dominated at more negative potentials (Fig. 3b,c). As demonstrated in Fig. 3d, CeO_2/CB generated exclusively H_2 with a very small amount of ECR products (FE < 3.0%). Although CuO/CB can reduce CO_2 at overpotentials larger than 0.97 V, the highest FE for ECR was below 32.0%, with the selectivity for C_{2+} products being less than 23.0%. Noteworthy is that the CuO/CeO_2 nanocomposites substantially promoted the activity toward CO_2 reduction with a FE > 63.0%. The C_1 products were obtained at similar yields for CuO/CB and $CuO\text{-}CeO_2/CB$, but C_{2+} products selectivity, C_2H_4 FE and production rate (Fig. 3e) were remarkably boosted on the latter sample. C_2H_4 emerged at an onset potential of –0.7 V (vs RHE) over $CuO\text{-}CeO_2/CB$ and rose to a maximum with FE up to 50.0% at −1.1 V (vs RHE), in contrast to that of 22.6% and 1.2% for CuO/CB, and CeO_2/CB, respectively (Fig. 3b,d). The C_2H_4 selectivity even outperforms many recently reported Cu-based electrocatalysts under similar overpotentials (Fig. 3f), such as state-of-the-art Cu nanocubes with exposed (100) facets (maximum C_2H_4 FE 32.0%),[44, 45] Ag-Cu nanodimers (maximum C_2H_4 FE 40.0%).[22]

The ECR activity was tunable by adjusting the amounts of CeO_2 and CuO. As seen in Fig. 3g, incorporation of CeO_2 at various contents was found to thwart hydrogen evolution and facilitate C_2H_4 generation. The optimal loading of CeO_2 was 30.0 wt%. Continuous increase in CeO_2 loading led to a slight activity decrease of ECR, probably owing to reduction in electrical conductivity. Likewise, the ECR activity to yield C_2H_4 increased with the mass percentage of CuO in the range from 0.75 to 1.5 wt%, above which the C_2H_4 FE tended to diminish upon further increase of the CuO loading (Fig. 3h). This may be due to a combination of less extended interface and formation of larger CuO particles, resulting in weakened binding of the reactants and intermediates. Furthermore, it was found that there is an optimum in the particle size of CuO which maximized C_2H_4 generation (Fig. S4), in line with the results observed for Cu in the literature.[22]

To check if Ce^{3+} impacted the ECR, the synthesis of catalysts was performed in an air-free glove-box under otherwise similar conditions. The resulting CuO-Ce_2O_3/CB provided a much lower C_2H_4 FE (22.4% at −1.1 V vs RHE) compared to CuO-CeO_2/CB. This indicates that Ce^{3+} is unlikely to contribute to the enhanced ECR.

The role of Cu^+ during ECR was investigated by treating CuO-CeO_2/CB at 200 °C under different atmospheres. As observed in Fig. 3i, the CO_2 reduction activity and selectivity remained almost unchanged in an Ar environment that may favor the transformation of a small fraction of Cu^{2+} to Cu^+, whereas the C_2H_4 FE slightly decreased with a simultaneous increase of CH_4 FE, probably resulting from aggregation of metal oxide NPs. This phenomenon became a little more pronounced after being subjected to water vapor, which may be due to promotion of CH_4 formation by the adsorbed surface water molecules. However, annealing of the catalyst in 8% H_2/Ar (to convert Cu^+ to Cu^0) led to increased HER with a distinct drop in ECR performance. Despite the CO FE being improved to 33.7%, the C_2H_4 FE fell down to 33.8%. This suggests that the reduction of Cu^+/Cu^0 ratio is detrimental to CO-CO coupling. Also, the reduction of Cu^+/Cu^{2+} by exposure of the sample to air at elevated temperature degraded C_2H_4 production, accompanied with substantially more H_2 evolution.

To probe the role of the CuO-CeO_2 interface, we made efforts to tailor the interfacial structure by fine-tuning of synthetic parameters such as the feeding sequence of metal precursors. When using a mixture of the two precursor solutions during catalyst synthesis, only 22.0% of C_2H_4 FE was attained (Fig. S5). Alternatively,

a cascade addition of copper precursor and cerium precursor in sequence also gave rise to a lower C_2H_4 FE of about 37.8%. In both cases, the accessible CuO-CeO_2 interfaces with exposed copper domains were markedly reduced, which accounted for the declined ECR performance. A physical mixture of CuO/CB and CeO_2/CB (CuO-CeO_2/CB_{mix}) with equivalent metal oxide loadings was also evaluated for ECR. It showed even worse CO_2 reduction activity than CuO/CB (Fig. 3d,e), most likely due to poor mass transport. Taken together, we conclude that intelligent design of CuO-CeO_2 interfaces to yield and stabilize Cu^+ is essential to facilitate CO_2-to-C_2H_4 conversion.

The interfacial reaction kinetics was explored by Tafel analysis. A Tafel slope of 148.9 mV dec^{-1} was observed for CuO-CeO_2/CB, much lower than 160.7 mV dec^{-1} for CuO/CB (Fig. 3j). This indicates that the CuO-CeO_2/CB has a comparatively faster kinetics for CO_2 reduction. The formation of the *CO intermediate for tandem catalysis on the surface of the catalysts determines the reaction rate.

The long-term performances of the catalysts were examined by chronoamperometric measurements. The results (Fig. 4f) showed that the FE for C_2H_4 remained steady slightly over 48.0% even after more than 10 h of continuous polarization at −1.1 V (vs RHE).

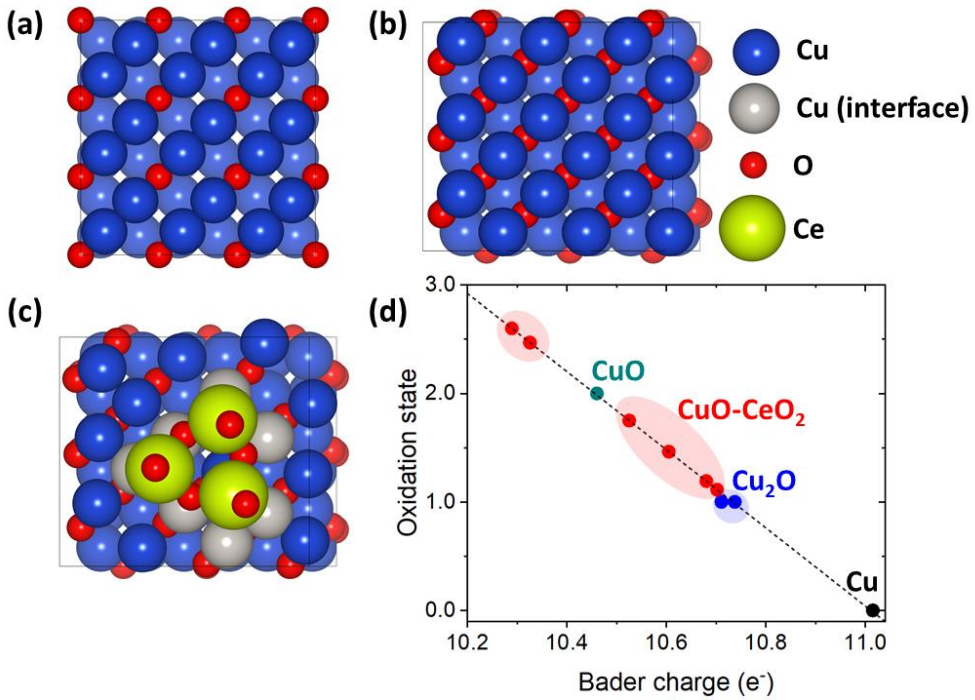

Figure 4. Top-view of the optimized geometries of (a) Cu_2O, (b) CuO and (c) CuO-CeO_2 and (d) oxidation states of surface Cu atoms obtained by Bader charge analysis. Only the surface Cu atoms adjacent to CeO_2 (denoted as grey balls in (c)) are considered for the Bader charge analysis

of CuO-CeO_2. In (d), black, blue, cyan and red colors represent Cu, Cu_2O, CuO and CuO-CeO_2, respectively.

To further investigate the role of CeO_2 in stabilizing Cu^+, we performed density functional theory (DFT) calculations (Fig. 4). We modeled the interface between CuO and CeO_2 (denoted as CuO-CeO_2) by constructing a small CeO_2 cluster (Ce_3O_6) on the CuO(100) surface.[46, 47] The (100) facet, which has been known as the active site for C_2 production in electrochemical CO_2 reduction, is considered.[48] We focus on the change/trend of the Bader charges[49] of the surface Cu atoms with and without CeO_2 cluster since the Bader charge agrees with the oxidation state qualitatively (albeit not quantitatively). Assuming that the Bader charges of surface Cu atoms in Cu(100), Cu_2O(100) and CuO(100) correspond to the oxidation states of 0, +1 and +2, respectively, we obtain a linear relationship between the Bader charge vs. oxidation state (Fig. 4d), and from the latter correlation we obtain the oxidation state of Cu atoms in CuO-CeO_2.

This Bader charge analysis shows that the oxidation states of several Cu atoms at the CuO-CeO_2 interface lie between that of Cu_2O and CuO (Fig. 4d), indicating that the interfacial CeO_2 cluster changes the oxidation state of neighboring Cu atoms in CuO toward that of Cu_2O. More specifically, oxidation states of two Cu atoms at the CuO-CeO_2 interface are highly similar to those of surface Cu atoms in Cu_2O (i.e. Cu^+). This result agrees with the presence of Cu^+ in the XPS characterization of CuO-CeO_2/CB (Fig. 1b) and indicates that the CeO_2 plays an important role in stabilizing Cu^+.

CONCLUSION

In summary, we present CuO-CeO_2/CB as a highly promising electrocatalyst for enhancing selective reduction of CO_2 to ethylene. By utilizing the strong synergistic interaction between CuO and CeO_2, stabilization of the Cu^+ species at the metal oxide interface is realized, while H_2 production is simultaneously considerably suppressed, resulting in enhanced ethylene production with a high FE of 50.0%. The existence of Cu^+ species was confirmed by XPS and Raman spectroscopy, as well as TPR, which are believed to be the adsorption as well as active sites for activation of CO_2 molecules. This work provides a simple way to enhance the conversion of CO_2 into ethylene, and it is hoped that the findings will inspire the rational design of active

copper domains for efficient electroreduction of CO_2.

Acknowledgements

This work was supported by National Natural Science Foundation of China (No. 21972010); the State Key Laboratory of Organic-Inorganic Composites (No. oic-201901001); Beijing Natural Science Foundation (No. 2192039); Beijing University of Chemical Technology (XK180301); the Foundation of Key Laboratory of Low-Carbon Conversion Science & Engineering, Shanghai Advanced Research Institute, Chinese Academy of Sciences (No. KLLCCSE-201901, SARI, CAS); the DCCEM at Department of Materials, Oxford, and the Henry Royce Institute (EP/R010145/1). Y.J. acknowledges the National Research Foundation of Korea (NRF-2019M3D1A1079303).

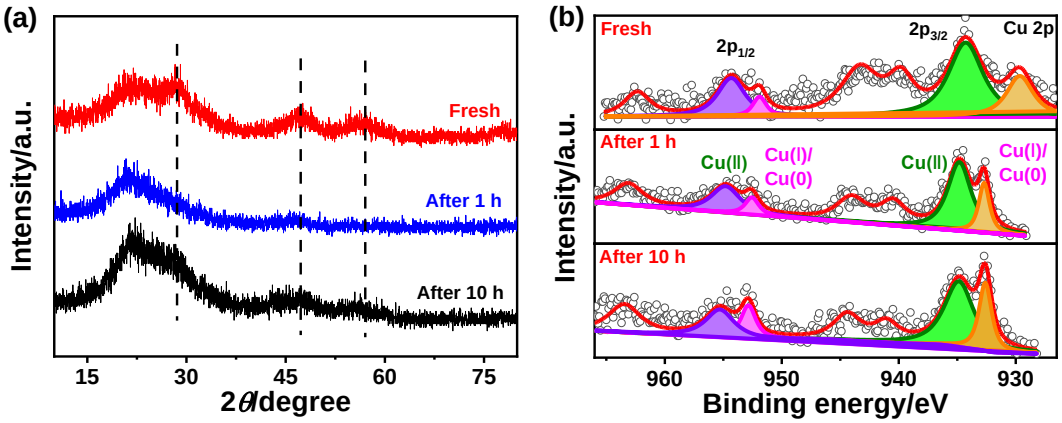

Fig. SI (a) (b) Cu 2p XPS spectra of CuO/CB and CuO-CeO_2/CB after CO_2 electroreduction catalysis.

References

1. Gu, J.; Hsu, C. S.; Bai, L. C.; Chen, H. M.; Hu, X., Atomically dispersed Fe^{3+} sites catalyze efficient CO_2 electroreduction to CO. *Science* **2019,** *364* (6445), 1091-1094.

2. Nitopi, S.; Bertheussen, E.; Scott, S. B.; Liu, X.; Engstfeld, A. K.; Horch, S.; Seger, B.; Stephens, I. E. L.; Chan, K.; Hahn, C.; Nørskov, J. K.; Chorkendorff, I., Progress and perspectives of electrochemical CO_2 reduction on copper in aqueous electrolyte. *Chem. Rev.* **2019,** *119* (12), 7610-7672.

3. Sun, Z. Y.; Ma, T.; Tao, H. C.; Fan, Q.; Han, B. X., Fundamentals and challenges of electrochemical CO_2 reduction using two-dimensional materials. *Chem* **2017,** *3* (4), 560-587.

4. Ma, T.; Fan, Q.; Li, X.; Qiu, J. S.; Wu, T. B.; Sun, Z. Y., Graphene-based materials for electrochemical CO_2 reduction. *J. CO_2 Util.* **2019,** *30*, 168-182.

5. Tao, H. c.; Fan, Q.; Ma, T.; Liu, S. z.; Gysling, H.; Texter, J.; Guo, F.; Sun, Z. y., Two-dimensional materials for energy conversion and storage. *Prog. Mater. Sci.* **2020**, 100637.

6. Fan, Q.; Hou, P. f.; Choi, C.; Wu, T. S.; Hong, S.; Li, F.; Soo, Y. L.; Kang, P.; Jung, Y. s.; Sun, Z. y., Activation of Ni Particles into Single Ni–N Atoms for Efficient Electrochemical Reduction of CO_2. *Adv. Energy Mater.* **2020,** *10* (5), 1903068.

7. Guan, A. x.; Chen, Z.; Quan, Y. l.; Peng, C.; Wang, Z. q.; Sham, T.-K.; Yang, C.; Ji, Y.; Qian, L. p.; Xu, X., Boosting CO_2 Electroreduction to CH_4 via Tuning Neighboring Single Copper Sites. *ACS Energy Lett.* **2020**.

8. Pi, Y. c.; Guo, J.; Shao, Q.; Huang, X. q., All-inorganic $SrSnO_3$ perovskite nanowires for efficient CO_2 electroreduction. *Nano Energy* **2019,** *62*, 861-868.

9. Yang, H. p.; Wu, Y.; Li, G. d.; Lin, Q.; Hu, Q.; Zhang, Q. l.; Liu, J. h.; He, C. x., Scalable production of efficient single-atom copper decorated carbon membranes for CO_2 electroreduction to methanol. *J. Am. Chem. Soc.* **2019,** *141* (32), 12717-12723.

10. Lv, J. J.; Jouny, M.; Luc, W.; Zhu, W. l.; Zhu, J. J.; Jiao, F., A highly porous copper electrocatalyst for carbon dioxide reduction. *Adv. Mater.* **2018,** *30* (49), 1803111.

11. Jia, M. W.; Choi, C.; Wu, T. S.; Ma, C.; Kang, P.; Tao, H. C.; Fan, Q.; Hong, S.; Liu, S. Z.; Soo, Y. L.; Sun, Z. Y., Carbon-supported Ni nanoparticles for efficient CO_2 electroreduction. *Chem. Sci.* **2018,** *9* (47), 8775-8780.

12. Jia, M. w.; Fan, Q.; Liu, S. z.; Qiu, J. s.; Sun, Z. y., Single-atom catalysis for electrochemical CO_2 reduction. *Curr. Opin. Green Sustainable Chem.* **2019,** *16*, 1-6.

13. Liu, S. b.; Lu, X. F.; Xiao, J.; Wang, X.; Lou, X. W., Bi_2O_3 Nanosheets Grown on Multi‐Channel Carbon Matrix to Catalyze Efficient CO_2 Electroreduction to HCOOH. *Angew. Chem. Int. Ed* **2019,** *58* (39), 13828-13833.

14. Gong, Q. f.; Ding, P.; Xu, M. q.; Zhu, X. r.; Wang, M. y.; Deng, J.; Ma, Q.; Han, N.; Zhu, Y.; Lu, J., Structural defects on converted bismuth oxide nanotubes enable highly active electrocatalysis of carbon dioxide reduction. *Nat. Commun.* **2019,** *10* (1), 1-10.

15. Xia, C.; Zhu, P.; Jiang, Q.; Pan, Y.; Liang, W. t.; Stavitsk, E.; Alshareef, H. N.; Wang, H., Continuous production of pure liquid fuel solutions via electrocatalytic CO_2 reduction using solid-electrolyte devices. *Nat. Energy* **2019,** *4* (9), 776-785.

16. Gao, D. f.; Zhou, H.; Cai, F.; Wang, J. g.; Wang, G. x.; Bao, X. h., Pd-containing nanostructures for electrochemical CO_2 reduction reaction. *ACS Catal.* **2018,** *8* (2), 1510-1519.

17. Fan, Q.; Zhang, M. L.; Jia, M. W.; Liu, S. Z.; Qiu, J. S.; Sun, Z. Y., Electrochemical CO_2 reduction to C_{2+} species: Heterogeneous electrocatalysts, reaction pathways, and optimization strategies. *Mater. Today Energy* **2018,** *10*, 280-301.

18. Gao, Y. N.; Liu, S. Z.; Zhao, Z. Q.; Tao, H. C.; Sun, Z. Y., Heterogeneous Catalysis of CO_2 Hydrogenation to C_{2+} Products. *Acta Phys. -Chim. Sin.* **2018,** *34* (8), 858-872.

19. Tao, M.; Qun, F.; Cong, T. H.; Shan, H. Z.; Wen, J. M.; Nan, G. Y.; Jing, M. W.; Yu, S. Z., Heterogeneous electrochemical CO_2 reduction using nonmetallic carbon-based catalysts: Current status and future challenges. *Nanotechnology* **2017,** *28*, 472001-472019.

20. Zhou, Y. s.; Che, F. l.; Liu, M.; Zou, C. q.; Liang, Z. q.; De Luna, P.; Yuan, H. f.; Li, J.; Wang, Z. q.; Xie, H. p., Dopant-induced electron localization drives CO_2 reduction to C_2 hydrocarbons. *Nat. Chem.* **2018,** *10* (9), 974-980.

21. Vasileff, A.; Xu, C. c.; Jiao, Y.; Zheng, Y.; Qiao, S.-Z., Surface and interface engineering in copper-based bimetallic materials for selective CO_2 electroreduction. *Chem* **2018,** *4* (8), 1809-1831.

22. Huang, J. F.; Mensi, M.; Oveisi, E.; Mantella, V.; Buonsanti, R., Structural Sensitivities in Bimetallic Catalysts for Electrochemical CO_2 Reduction Revealed by Ag–Cu Nanodimers. *J. Am. Chem. Soc.* **2019,** *141* (6), 2490-2499.

23. Hori, Y.; Takahashi, I.; Koga, O.; Hoshi, N., Electrochemical reduction of carbon dioxide at various series of copper single crystal electrodes. *J. Mol. Catal. A Chem.* **2003,** *199* (1-2), 39-47.

24. Wu, Y. A.; McNulty, I.; Liu, C.; Lau, K. C.; Liu, Q.; Paulikas, A. P.; Sun, C.-J.; Cai, Z. h.; Guest, J. R.; Ren, Y., Facet-dependent active sites of a single Cu_2O particle photocatalyst for CO_2 reduction to methanol. *Nat. Energy* **2019,** *4* (11), 957-968.

25. Lee, S. Y.; Jung, H.; Kim, N. K.; Oh, H. S.; Min, B. K.; Hwang, Y. J., Mixed copper states in anodized Cu electrocatalyst for stable and selective ethylene production from CO_2 reduction. *J. Am. Chem. Soc.* **2018,** *140* (28), 8681-8689.

26. Jung, H.; Lee, S. Y.; Lee, C. W.; Cho, M. K.; Won, D. H.; Kim, C.; Oh, H.-S.; Min, B. K.; Hwang, Y. J., Electrochemical Fragmentation of Cu_2O Nanoparticles Enhancing Selective C–C Coupling from CO_2 Reduction Reaction. *J. Am. Chem. Soc.* **2019,** *141* (11), 4624-4633.

27. Luc, W.; Fu, X. b.; Shi, J. j.; Lv, J.-J.; Jouny, M.; Ko, B. H.; Xu, Y. b.; Tu, Q.; Hu, X. b.; Wu, J. s., Two-dimensional copper nanosheets for electrochemical reduction of carbon monoxide to acetate. *Nat. Catal.* **2019,** *2* (5), 423-430.

28. Nam, D.-H.; Bushuyev, O. S.; Li, J.; De Luna, P.; Seifitokaldani, A.; Dinh, C.-T.; García de

Arquer, F. P.; Wang, Y. h.; Liang, Z. q.; Proppe, A. H., Metal–Organic Frameworks Mediate Cu Coordination for Selective CO_2 Electroreduction. *J. Am. Chem. Soc.* **2018,** *140* (36), 11378-11386.

29. De Luna, P.; Quintero Bermudez, R.; Dinh, C. T.; Ross, M. B.; Bushuyev, O. S.; Todorović, P.; Regier, T.; Kelley, S. O.; Yang, P. d.; Sargent, E. H., Catalyst electro-redeposition controls morphology and oxidation state for selective carbon dioxide reduction. *Nat. Catal.* **2018,** *1* (2), 103-110.

30. Hori, Y.; Takahashi, I.; Koga, O.; Hoshi, N., Electrochemical reduction of carbon dioxide at various series of copper single crystal electrodes. *J. Mol. Catal. A Chem.* **2003,** *199* (1-2), 39-47.

31. Clark, E. L.; Hahn, C.; Jaramillo, T. F.; Bell, A. T., Electrochemical CO_2 reduction over compressively strained CuAg surface alloys with enhanced multi-carbon oxygenate selectivity. *J. Am. Chem. Soc.* **2017,** *139* (44), 15848-15857.

32. Chu, S. L.; Hong, S.; Masa, J.; Li, X.; Sun, Z. Y., Synergistic Catalysis of CuO/In_2O_3 Composites for Highly Selective Electrochemical CO_2 Reduction to CO. *Chem. Commun.* **2019,** *55*, 12380-12383.

33. Li, Y. m.; Chu, S. l.; Shen, H. d.; Xia, Q. n.; Robertson, A. W.; Masa, J.; Siddiqui, U.; Sun, Z. y., Achieving highly selective electrocatalytic CO_2 reduction by tuning $CuO\text{-}Sb_2O_3$ nanocomposites. *ACS Sustainable Chem. Eng.* **2020**.

34. Favaro, M.; Xiao, H.; Cheng, T.; Goddard, W. A.; Yano, J.; Crumlin, E. J., Subsurface oxide plays a critical role in CO_2 activation by Cu (111) surfaces to form chemisorbed CO_2, the first step in reduction of CO_2. *Proc. Natl Acd. Sci.* **2017,** *114* (26), 6706-6711.

35. Xiao, H.; Goddard, W. A.; Cheng, T.; Liu, Y., Cu metal embedded in oxidized matrix catalyst to promote CO_2 activation and CO dimerization for electrochemical reduction of CO_2. *Proc. Natl Acd. Sci.* **2017,** *114* (26), 6685-6688.

36. Lei, Q.; Zhu, H.; Song, K. p.; Wei, N. n.; Liu, L. m.; Zhang, D. l.; Yin, J.; Dong, X. l.; Yao, K. x.; Wang, N., Investigating the Origin of Enhanced C_{2+} Selectivity in Oxide-/Hydroxide-derived Copper Electrodes during CO_2 Electroreduction. *J. Am. Chem. Soc.* **2020,** *142*, 4213.

37. Burroughs, P.; Hamnett, A.; Orchard, A. F.; Thornton, G., Satellite structure in the X-ray photoelectron spectra of some binary and mixed oxides of lanthanum and cerium. *J. Chem. Soc., Dalton Trans.* **1976,** (17), 1686-1698.

38. Sun, Z. Y.; Wang, X.; Liu, Z. M.; Zhang, H. Y.; Yu, P.; Mao, L. Q., Pt− Ru/CeO_2/carbon nanotube nanocomposites: an efficient electrocatalyst for direct methanol fuel cells. *Langmuir* **2010,** *26* (14), 12383-12389.

39. Han, Z. S.; Choi, C.; Tao, H. C.; Fan, Q.; Gao, Y. N.; Liu, S. Z.; Robertson, A. W.; Hong, S.; Jung, Y. S.; Sun, Z. Y., Tuning the Pd-catalyzed electroreduction of CO_2 to CO with reduced overpotential. *Catal. Sci. Technol.* **2018,** *8* (15), 3894-3900.

40. Shyu, J.; Otto, K.; Watkins, W.; Graham, G.; Belitz, R.; Gandhi, H., Characterization of Pd/γ-alumina catalysts containing ceria. *J. Catal.* **1988,** *114* (1), 23-33.

41. Spanier, J. E.; Robinson, R. D.; Zhang, F.; Chan, S.-W.; Herman, I. P., Size-dependent properties of $CeO_{2-\gamma}$ nanoparticles as studied by Raman scattering. *Phys. Rev. B* **2001,** *64* (24), 245407.

42. Hagemann, H.; Bill, H.; Walker, E.; François, M., Raman spectra of single crystal CuO. *Solid State Commun.* **1990,** *73* (6), 447-451.

43. Zhang, M. L.; Wu, T. S.; Hong, S.; Fan, Q.; Soo, Y. L.; Masa, J.; Qiu, J. S.; Sun, Z. Y., Efficient Electrochemical Reduction of CO_2 by Ni–N Catalysts with Tunable Performance. *ACS Sustainable Chem. Eng.* **2019,** *7* (17), 15030-15035.

44. Loiudice, A.; Lobaccaro, P.; Kamali, E. A.; Thao, T.; Huang, B. H.; Ager, J. W.; Buonsanti,

R., Tailoring copper nanocrystals towards C_2 products in electrochemical CO_2 reduction. *Angew. Chem. Int. Ed* **2016,** *55* (19), 5789-5792.

45. Jiang, K.; Sandberg, R. B.; Akey, A. J.; Liu, X. y.; Bell, D. C.; Nørskov, J. K.; Chan, K.; Wang, H., Metal ion cycling of Cu foil for selective C–C coupling in electrochemical CO_2 reduction. *Nat. Catal.* **2018,** *1* (2), 111-119.

1. Gu, J.; Hsu, C. S.; Bai, L. C.; Chen, H. M.; Hu, X., Atomically dispersed Fe^{3+} sites catalyze efficient CO_2 electroreduction to CO. *Science* **2019,** *364* (6445), 1091-1094.

2. Nitopi, S.; Bertheussen, E.; Scott, S. B.; Liu, X.; Engstfeld, A. K.; Horch, S.; Seger, B.; Stephens, I. E. L.; Chan, K.; Hahn, C.; Nørskov, J. K.; Chorkendorff, I., Progress and perspectives of electrochemical CO_2 reduction on copper in aqueous electrolyte. *Chem. Rev.* **2019,** *119* (12), 7610-7672.

3. Sun, Z. Y.; Ma, T.; Tao, H. C.; Fan, Q.; Han, B. X., Fundamentals and challenges of electrochemical CO_2 reduction using two-dimensional materials. *Chem* **2017,** *3* (4), 560-587.

4. Ma, T.; Fan, Q.; Li, X.; Qiu, J. S.; Wu, T. B.; Sun, Z. Y., Graphene-based materials for electrochemical CO_2 reduction. *J. CO_2 Util.* **2019,** *30*, 168-182.

5. Tao, H. c.; Fan, Q.; Ma, T.; Liu, S. z.; Gysling, H.; Texter, J.; Guo, F.; Sun, Z. y., Two-dimensional materials for energy conversion and storage. *Prog. Mater. Sci.* **2020**, 100637.

6. Fan, Q.; Hou, P. f.; Choi, C.; Wu, T. S.; Hong, S.; Li, F.; Soo, Y. L.; Kang, P.; Jung, Y. s.; Sun, Z. y., Activation of Ni Particles into Single Ni–N Atoms for Efficient Electrochemical Reduction of CO_2. *Adv. Energy Mater.* **2020,** *10* (5), 1903068.

7. Guan, A. x.; Chen, Z.; Quan, Y. l.; Peng, C.; Wang, Z. q.; Sham, T.-K.; Yang, C.; Ji, Y.; Qian, L. p.; Xu, X., Boosting CO_2 Electroreduction to CH_4 via Tuning Neighboring Single Copper Sites. *ACS Energy Lett.* **2020**.

8. Pi, Y. c.; Guo, J.; Shao, Q.; Huang, X. q., All-inorganic $SrSnO_3$ perovskite nanowires for efficient CO_2 electroreduction. *Nano Energy* **2019,** *62*, 861-868.

9. Yang, H. p.; Wu, Y.; Li, G. d.; Lin, Q.; Hu, Q.; Zhang, Q. l.; Liu, J. h.; He, C. x., Scalable production of efficient single-atom copper decorated carbon membranes for CO_2 electroreduction to methanol. *J. Am. Chem. Soc.* **2019,** *141* (32), 12717-12723.

10. Lv, J. J.; Jouny, M.; Luc, W.; Zhu, W. l.; Zhu, J. J.; Jiao, F., A highly porous copper electrocatalyst for carbon dioxide reduction. *Adv. Mater.* **2018,** *30* (49), 1803111.

11. Jia, M. W.; Choi, C.; Wu, T. S.; Ma, C.; Kang, P.; Tao, H. C.; Fan, Q.; Hong, S.; Liu, S. Z.; Soo, Y. L.; Sun, Z. Y., Carbon-supported Ni nanoparticles for efficient CO_2 electroreduction. *Chem. Sci.* **2018,** *9* (47), 8775-8780.

12. Jia, M. w.; Fan, Q.; Liu, S. z.; Qiu, J. s.; Sun, Z. y., Single-atom catalysis for electrochemical CO_2 reduction. *Curr. Opin. Green Sustainable Chem.* **2019,** *16*, 1-6.

13. Liu, S. b.; Lu, X. F.; Xiao, J.; Wang, X.; Lou, X. W., Bi_2O_3 Nanosheets Grown on Multi‐Channel Carbon Matrix to Catalyze Efficient CO_2 Electroreduction to HCOOH. *Angew. Chem. Int. Ed* **2019,** *58* (39), 13828-13833.

14. Gong, Q. f.; Ding, P.; Xu, M. q.; Zhu, X. r.; Wang, M. y.; Deng, J.; Ma, Q.; Han, N.; Zhu, Y.; Lu, J., Structural defects on converted bismuth oxide nanotubes enable highly active electrocatalysis of carbon dioxide reduction. *Nat. Commun.* **2019,** *10* (1), 1-10.

15. Xia, C.; Zhu, P.; Jiang, Q.; Pan, Y.; Liang, W. t.; Stavitsk, E.; Alshareef, H. N.; Wang, H., Continuous production of pure liquid fuel solutions via electrocatalytic CO_2 reduction using solid-electrolyte devices. *Nat. Energy* **2019,** *4* (9), 776-785.

16. Gao, D. f.; Zhou, H.; Cai, F.; Wang, J. g.; Wang, G. x.; Bao, X. h., Pd-containing nanostructures for electrochemical CO_2 reduction reaction. *ACS Catal.* **2018,** *8* (2), 1510-1519.

17. Fan, Q.; Zhang, M. L.; Jia, M. W.; Liu, S. Z.; Qiu, J. S.; Sun, Z. Y., Electrochemical CO_2 reduction to C_{2+} species: Heterogeneous electrocatalysts, reaction pathways, and optimization strategies. *Mater. Today Energy* **2018,** *10*, 280-301.

18. Gao, Y. N.; Liu, S. Z.; Zhao, Z. Q.; Tao, H. C.; Sun, Z. Y., Heterogeneous Catalysis of CO_2 Hydrogenation to C_{2+} Products. *Acta Phys. -Chim. Sin.* **2018,** *34* (8), 858-872.

19. Tao, M.; Qun, F.; Cong, T. H.; Shan, H. Z.; Wen, J. M.; Nan, G. Y.; Jing, M. W.; Yu, S. Z., Heterogeneous electrochemical CO_2 reduction using nonmetallic carbon-based catalysts: Current status and future challenges. *Nanotechnology* **2017,** *28*, 472001-472019.

20. Zhou, Y. s.; Che, F. l.; Liu, M.; Zou, C. q.; Liang, Z. q.; De Luna, P.; Yuan, H. f.; Li, J.; Wang, Z. q.; Xie, H. p., Dopant-induced electron localization drives CO_2 reduction to C_2 hydrocarbons. *Nat. Chem.* **2018,** *10* (9), 974-980.

21. Vasileff, A.; Xu, C. c.; Jiao, Y.; Zheng, Y.; Qiao, S.-Z., Surface and interface engineering in copper-based bimetallic materials for selective CO_2 electroreduction. *Chem* **2018,** *4* (8), 1809-1831.

22. Huang, J. F.; Mensi, M.; Oveisi, E.; Mantella, V.; Buonsanti, R., Structural Sensitivities in Bimetallic Catalysts for Electrochemical CO_2 Reduction Revealed by Ag–Cu Nanodimers. *J. Am. Chem. Soc.* **2019,** *141* (6), 2490-2499.

23. Hori, Y.; Takahashi, I.; Koga, O.; Hoshi, N., Electrochemical reduction of carbon dioxide at various series of copper single crystal electrodes. *J. Mol. Catal. A Chem.* **2003,** *199* (1-2), 39-47.

24. Wu, Y. A.; McNulty, I.; Liu, C.; Lau, K. C.; Liu, Q.; Paulikas, A. P.; Sun, C.-J.; Cai, Z. h.; Guest, J. R.; Ren, Y., Facet-dependent active sites of a single Cu_2O particle photocatalyst for CO_2 reduction to methanol. *Nat. Energy* **2019,** *4* (11), 957-968.

25. Lee, S. Y.; Jung, H.; Kim, N. K.; Oh, H. S.; Min, B. K.; Hwang, Y. J., Mixed copper states in anodized Cu electrocatalyst for stable and selective ethylene production from CO_2 reduction. *J. Am. Chem. Soc.* **2018,** *140* (28), 8681-8689.

26. Jung, H.; Lee, S. Y.; Lee, C. W.; Cho, M. K.; Won, D. H.; Kim, C.; Oh, H.-S.; Min, B. K.; Hwang, Y. J., Electrochemical Fragmentation of Cu_2O Nanoparticles Enhancing Selective C–C Coupling from CO_2 Reduction Reaction. *J. Am. Chem. Soc.* **2019,** *141* (11), 4624-4633.

27. Luc, W.; Fu, X. b.; Shi, J. j.; Lv, J.-J.; Jouny, M.; Ko, B. H.; Xu, Y. b.; Tu, Q.; Hu, X. b.; Wu, J. s., Two-dimensional copper nanosheets for electrochemical reduction of carbon monoxide to acetate. *Nat. Catal.* **2019,** *2* (5), 423-430.

28. Nam, D.-H.; Bushuyev, O. S.; Li, J.; De Luna, P.; Seifitokaldani, A.; Dinh, C.-T.; García de Arquer, F. P.; Wang, Y. h.; Liang, Z. q.; Proppe, A. H., Metal–Organic Frameworks Mediate Cu Coordination for Selective CO_2 Electroreduction. *J. Am. Chem. Soc.* **2018,** *140* (36), 11378-11386.

29. De Luna, P.; Quintero Bermudez, R.; Dinh, C. T.; Ross, M. B.; Bushuyev, O. S.; Todorović, P.; Regier, T.; Kelley, S. O.; Yang, P. d.; Sargent, E. H., Catalyst electro-redeposition controls morphology and oxidation state for selective carbon dioxide reduction. *Nat. Catal.* **2018,** *1* (2), 103-110.

30. Hori, Y.; Takahashi, I.; Koga, O.; Hoshi, N., Electrochemical reduction of carbon dioxide at various series of copper single crystal electrodes. *J. Mol. Catal. A Chem.* **2003,** *199* (1-2), 39-47.

31. Clark, E. L.; Hahn, C.; Jaramillo, T. F.; Bell, A. T., Electrochemical CO_2 reduction over compressively strained CuAg surface alloys with enhanced multi-carbon oxygenate selectivity. *J. Am. Chem. Soc.* **2017,** *139* (44), 15848-15857.

32. Chu, S. L.; Hong, S.; Masa, J.; Li, X.; Sun, Z. Y., Synergistic Catalysis of CuO/In_2O_3 Composites for Highly Selective Electrochemical CO_2 Reduction to CO. *Chem. Commun.* **2019,** *55*, 12380-12383.

33. Li, Y. m.; Chu, S. l.; Shen, H. d.; Xia, Q. n.; Robertson, A. W.; Masa, J.; Siddiqui, U.; Sun, Z. y., Achieving highly selective electrocatalytic CO_2 reduction by tuning CuO-Sb_2O_3 nanocomposites. *ACS Sustainable Chem. Eng.* **2020**.

34. Favaro, M.; Xiao, H.; Cheng, T.; Goddard, W. A.; Yano, J.; Crumlin, E. J., Subsurface oxide plays a critical role in CO_2 activation by Cu (111) surfaces to form chemisorbed CO_2, the first step in reduction of CO_2. *Proc. Natl Acd. Sci.* **2017,** *114* (26), 6706-6711.

35. Xiao, H.; Goddard, W. A.; Cheng, T.; Liu, Y., Cu metal embedded in oxidized matrix catalyst to promote CO_2 activation and CO dimerization for electrochemical reduction of CO_2. *Proc. Natl Acd. Sci.* **2017,** *114* (26), 6685-6688.

36. Lei, Q.; Zhu, H.; Song, K. p.; Wei, N. n.; Liu, L. m.; Zhang, D. l.; Yin, J.; Dong, X. l.; Yao, K. x.; Wang, N., Investigating the Origin of Enhanced C_{2+} Selectivity in Oxide-/Hydroxide-derived Copper Electrodes during CO_2 Electroreduction. *J. Am. Chem. Soc.* **2020,** *142*, 4213.

37. Burroughs, P.; Hamnett, A.; Orchard, A. F.; Thornton, G., Satellite structure in the X-ray photoelectron spectra of some binary and mixed oxides of lanthanum and cerium. *J. Chem. Soc., Dalton Trans.* **1976,** (17), 1686-1698.

38. Sun, Z. Y.; Wang, X.; Liu, Z. M.; Zhang, H. Y.; Yu, P.; Mao, L. Q., Pt− Ru/CeO_2/carbon nanotube nanocomposites: an efficient electrocatalyst for direct methanol fuel cells. *Langmuir* **2010,** *26* (14), 12383-12389.

39. Han, Z. S.; Choi, C.; Tao, H. C.; Fan, Q.; Gao, Y. N.; Liu, S. Z.; Robertson, A. W.; Hong, S.; Jung, Y. S.; Sun, Z. Y., Tuning the Pd-catalyzed electroreduction of CO_2 to CO with reduced overpotential. *Catal. Sci. Technol.* **2018,** *8* (15), 3894-3900.

40. Shyu, J.; Otto, K.; Watkins, W.; Graham, G.; Belitz, R.; Gandhi, H., Characterization of Pd/γ-alumina catalysts containing ceria. *J. Catal.* **1988,** *114* (1), 23-33.

41. Spanier, J. E.; Robinson, R. D.; Zhang, F.; Chan, S.-W.; Herman, I. P., Size-dependent properties of CeO_{2-y} nanoparticles as studied by Raman scattering. *Phys. Rev. B* **2001,** *64* (24), 245407.

42. Hagemann, H.; Bill, H.; Walker, E.; François, M., Raman spectra of single crystal CuO. *Solid State Commun.* **1990,** *73* (6), 447-451.

43. Zhang, M. L.; Wu, T. S.; Hong, S.; Fan, Q.; Soo, Y. L.; Masa, J.; Qiu, J. S.; Sun, Z. Y., Efficient Electrochemical Reduction of CO_2 by Ni–N Catalysts with Tunable Performance. *ACS Sustainable Chem. Eng.* **2019,** *7* (17), 15030-15035.

44. Loiudice, A.; Lobaccaro, P.; Kamali, E. A.; Thao, T.; Huang, B. H.; Ager, J. W.; Buonsanti, R., Tailoring copper nanocrystals towards C_2 products in electrochemical CO_2 reduction. *Angew. Chem. Int. Ed* **2016,** *55* (19), 5789-5792.

45. Jiang, K.; Sandberg, R. B.; Akey, A. J.; Liu, X. y.; Bell, D. C.; Nørskov, J. K.; Chan, K.; Wang, H., Metal ion cycling of Cu foil for selective C–C coupling in electrochemical CO_2 reduction. *Nat. Catal.* **2018,** *1* (2), 111-119.

46. Lee, C. W.; Shin, S.-J.; Jung, H.; Nguyen, D. L. T.; Lee, S. Y.; Lee, W. H.; Won, D. H.; Kim, M. G.; Oh, H.-S.; Jang, T., Metal–oxide interfaces for selective electrochemical C–C coupling reactions. *ACS Energy Lett.* **2019,** *4* (9), 2241-2248.

47. Gao, D.; Zhang, Y.; Zhou, Z.; Cai, F.; Zhao, X.; Huang, W.; Li, Y.; Zhu, J.; Liu, P.; Yang, F., Enhancing CO_2 electroreduction with the metal–oxide interface. *J. Am. Chem. Soc.* **2017,** *139* (16), 5652-5655.

48. Schouten, K. J. P.; Qin, Z.; Pérez Gallent, E.; Koper, M. T., Two pathways for the formation of ethylene in CO reduction on single-crystal copper electrodes. *J. Am. Chem. Soc.* **2012,** *134* (24), 9864-9867.

49. Tang, W.; Sanville, E.; Henkelman, G., A grid-based Bader analysis algorithm without lattice bias. *J. Phys.: Condens. Matter* **2009,** *21* (8), 084204.